Modeling characteristic curves of solar cells and optical detectors with the Simmon–Taylor approximation

M.G. De Greef [a,*], F.A. Rubinelli [a], Rene van Swaaij [b]

[a] INTEC, Universidad Nacional del Litoral, Güemes 3450, Santa Fe 3000, Argentina
[b] Delft University of Technology, Photovoltaic Materials and Devices – ESE, P. O. Box 5031, NL-2600 GA, Delft, The Netherlands

ARTICLE INFO

ABSTRACT

The performance of amorphous and microcrystalline silicon based electronic devices is highly dependent on the density of states present in the band gap. The density of states in these materials contains two exponentially decreasing tails and a high number of deep states. Charge trapping and the recombination of electron–hole pairs through gap states are usually described by the Schockley–Read–Hall (SRH) formalism. The equations derived in the SRH formalism can be highly simplified by using the Simmons–Taylor's algorithms, especially the one so called "0 K" approximation, which allows a quasi-analytical derivation of the current–voltage characteristics. Although the validity of these algorithms were discussed in the literature on semiconductor materials, there is not a systematic study where these algorithms were included in a computer code that numerically solves the governing semiconductor device equations in order to compare the characteristic curves predicted by these simplifications with the ones obtained with the SRH formalism. This paper is an attempt to fill this void. The approximations of Simmon–Taylor were implemented in our code D-AMPS and the current–voltage and spectral response curves were evaluated under different conditions: with and without bias light, at forward and reverse bias voltages, at different temperatures, for various intrinsic layer thicknesses and for different key electrical parameters. To simplify the discussion we have assumed a uniform density of states along the intrinsic layer. Our results indicate that the Simmon–Taylor approximation is acceptable when the device is working under illumination. Under dark conditions the approximation is also satisfactory when the device is forward biased but slightly overestimates the dark current when the device is reverse forward. Although the 0 K approximation leads us to unacceptable results when the device is reversed biased and operates under dark conditions it can also be used in device modeling taking some precautions.

© 2013 Elsevier B.V. All rights reserved.

1. Introduction

Amorphous materials do not show long-range structural order like their crystalline counterparts. Their atoms, at best, display only short-range order that produce the semiconducting properties. Small deviations in bond angles and lengths result in a random disordered network. Particularly in hydrogenated amorphous silicon (a-Si:H) defects are present in the form of silicon atoms with only three covalent bonds connected to their neighbors. The fourth bond is hanging and is usually called a Dangling Bond (DB). Instead of the sharply defined edges like for crystalline materials, two exponential tails extend into the band gap. Amorphous solids are described by a band picture with a large density of localized gap states: intrinsic states are composed of tail states that are more numerous near the band edges and by DB or deep states that are more numerous near mid gap. Extrinsic localized states are created by impurities. The description of the electrical transport is highly simplified by the concept of conduction and valence band mobility edges that define the mobility gap and separate extended states from localized states. Microcrystalline silicon (μc-Si:H) is a material that contains two solid phases: small volumes (in the order of 10 nm of diameter) of crystalline material embedded in an amorphous network being the fraction of crystalline material dependent of the deposition conditions. The density of gap states also contains two exponentially decaying tails and deep states that are usually described in both materials with Gaussian distributions.

The performance of amorphous and microcrystalline silicon based electronic devices is highly dependent on the density of gap states. The quasi-continuous density of states present in these materials highly influences the trapping and recombination of free carriers. The electric field, that separates the generated free carriers, is seriously altered by trapping that in turn impacts in the recombination rates. The electric field profile of a device under operation can depart from its shape at thermodynamic equilibrium by injection of carriers through contacts or by electron–hole (e–h) pair generation by illumination. Hence, careful evaluation of charge trapping, recombination rates, and the electric field is essential to accurately describe and model these devices.

* Corresponding author. Tel.: +54 342 4559175; fax: +54 342 450944.
E-mail address: mdegreef@santafe-conicet.gov.ar (M.G. De Greef).

In disordered semiconductors the total trapped charge density and the recombination rate can be computed by integrating over all gap states present between the band edges using the conventional Schockley–Read–Hall (SRH) model that was developed for crystalline semiconductors where usually only few discrete energy levels control recombination [1]. The SRH model describes charge trapping and re-combination processes using simple electron traps. Simmons and Taylor derived an elegant approximation (STA) [2] of the SRH formal-ism reducing the corresponding equations to much simpler expres-sions. This simplicity usually makes the physical interpretation of results obtained with the simulations easier. The so called "0 K" (0KSTA) approximation was widely used in solar cell modeling be-cause the analysis of the characteristic curves could be sometimes reduced to simple analytical models [3].

Although the goodness of these approximations has been discussed in semiconductor materials [1,4–6] we could not find a discussion in the literature where the errors introduced by these simplifications were quantified directly in electronic devices using numerical computer codes. In this paper we compare in single and double injection electron-ic devices the results obtained with our computer code D-AMPS [7] when either the SRH formalism or the algorithms derived in the STA and the 0KSTA are used to calculate the trapped charge densities and the recombination rate. The device characteristic curves are initially fitted with D-AMPS using the SRH algorithm. The STA and 0KSTA ap-proximations are tested with respect to the results obtained with the SRH formalism that will be used as our reference in this paper. The cur-rent voltage (J–V) and Spectral Responses (SR) of solar cells and optical detectors were evaluated for different scenarios.

Our paper is organized as follows: in Section 2 we briefly describe the SRH statistic and the Simmons–Taylor approximations; in Section 3 we describe the main features of our computer code D-AMPS and show our fittings of p–i–n a-Si:H and μc-Si:H based solar-cell characteristics; in Section 4 we discuss the results obtained with D-AMPS when the STA and 0KSTA approximations are implemented; and finally we move to our conclusions. We will soon submit an additional contribution where the impact of these approximations are discussed when the Defect Pool Model (DPM) is invoked in the description of the density of DB in a-Si:H devices. In the current paper we focus our effort in discussing results of general applicability not only for a-Si:H-based semiconductor devices but also for μc-Si:H structures. On the top as the STA was developed for decoupled (donor-like and acceptor-like) gap states and the DPM was derived for amphoteric-like gap states. This use of decoupled states within the DPM requires a separate discussion.

2. Short description of the statistic and the approximations

2.1. Shockley–Read–Hall statistic

In the theory developed by Shockley, Read and Hall [8,9] (SRH) four basic processes, characterized by their respective rates r_i, compete in order to define the occupation function f at the gap state located at the energy E_t: (1) electron capture from the conduction band (r_1), (2) electron emission to the conduction band (r_2), (3) hole capture from the valence band (r_3) and (4) hole emission to the valence band (r_4). The SRH theory assumes decoupled gap states; i.e. they could behave as either donor-like or acceptor-like traps. The equations in our paper will be expressed in general terms without specifying the charge state of traps in cross-sections and emission coefficients for donor and acceptor states.

The four processes are illustrated in Fig. 1 and theirs rates are listed in Table 1, where n and p are the free carrier concentrations, v_{th} is the thermal velocity, N_t is the trap density, f^n and $f^p = 1 - f^n$ are the occupation function for electrons and holes, σ_n and σ_p are the electron and hole capture cross-sections, and finally e_n and e_p are the emission coefficients for electrons and holes respectively. At thermal equilibrium no net recombination occurs so $r_1 = r_2$ and
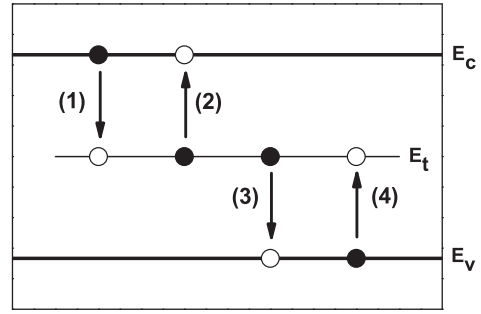

Fig. 1. Schematic illustration of the capture and emission processes of the SRH formal-ism for a single trap. E_C and E_V are the conduction band edges. The rates of these processes are listed in Table 1.

$r_3 = r_4$ (see Table 1). Using the Fermi–Dirac statistics valid at thermal equilibrium the emission rates (r_2 and r_4) can be expressed as:

$$e_n = v_{th}\sigma_n N_c \exp\left(\frac{E_t - E_c}{kT}\right) \quad (1)$$

$$e_p = v_{th}\sigma_p N_v \exp\left(\frac{E_v - E_t}{kT}\right) \quad (2)$$

where E_C and E_V are the conduction and valence band edges. Under non-equilibrium and at steady-state conditions the recombination process involves one electron and one hole, so the recombination rate is given by $R = r_1 - r_2 = r_3 - r_4$. From these equations the follow-ing expressions for the steady-state occupation functions and the re-combination rate (cm^{-3} s^{-1} eV^{-1}) can be obtained at a gap state of energy E_t:

$$f^n(E_t) = \frac{n v_{th}\sigma_n + e_p}{n v_{th}\sigma_n + p v_{th}\sigma_p + e_n + e_p} \quad (3a)$$

$$f^p(E_t) = 1 - f^n(E_t) = \frac{p v_{th}\sigma_p + e_n}{n v_{th}\sigma_n + p v_{th}\sigma_p + e_n + e_p} \quad (3b)$$

$$R(E_t) = N_t v_{th}^2 \sigma_n \sigma_p \frac{np - n_i^2}{n v_{th}\sigma_n + p v_{th}\sigma_p + e_n + e_p} \quad (4)$$

where n_i is the intrinsic carrier concentration.

The trapped charge residing at the gap state (C cm^{-3} eV^{-1}) of en-ergy E_t is given by the product of the trap density N_t, the correspond-ing occupation function and the electron charge. The expressions for acceptor- and donor-like states are respectively:

$$\rho_A(E_t) = -q N_t f^n(E_t) \quad (5)$$

$$\rho_D(E_t) = +q N_t f^p(E_t) \quad (6)$$

In disordered semiconductors the total trapped charge density ρ (C cm^{-3}) and the total recombination rate R (cm^{-3} s^{-1} eV^{-1}) can be computed by integrating the expressions (5–6) over all the gap states.

Table 1
Processes associated with single-electron trapping, and their rates.

	Process	Rate
1	Electron capture	$r_1 = n v_{th} \sigma_n N_t (1 - f)$
2	Electron emission	$r_2 = e_n N_t f$
3	Hole capture	$r_3 = p v_{th} \sigma_n N_t f$
4	Hole emission	$r_4 = e_p N_t (1 - f)$

2.2. Simmons–Taylor approximation (STA)

The STA has been derived for materials containing a continuous distribution of gap states. The authors define the trap class R_σ where all traps have identical electron and hole cross-sections independently of their energy. If there are more than one species of traps the approximation can be applied to each class of traps and the total recombination and space charge density can be obtained by summing up the contributions of the different species. In our case the different species correspond to the states of the conduction band tail, the valence band tail and the Gaussians distributions used to represent deep states.

Simmons and Taylor defined the intrinsic trap level, E_{T0}, as the energy where the emission rates of electrons to the conduction band and holes to the valence band are equal; i.e. $e_n(E_{T0}) = e_p(E_{T0})$. Since the emission rates exponentially increase or decrease with the trap energy E_t either e_n or e_p can be neglected few kT away from E_{T0}. Using this argument the electron and hole occupation functions can be rewritten as [3]:

$$f^n(E_t) = \frac{n\sigma_n}{n\sigma_n + p\sigma_p}\left[1 + \exp\left(\frac{E_t - E_{fnt}}{kT}\right)\right]^{-1} \text{ for } E_t > E_{t0} \quad (7)$$

$$f^p(E_t) = 1 - f^n(E_t) = \frac{p\sigma_p}{n\sigma_n + p\sigma_p}\left[1 + \exp\left(\frac{E_{fpt} - E_t}{kT}\right)\right]^{-1} \text{ for } E_t < E_{t0} \quad (8)$$

where E_{fnt} and E_{fpt} are the quasi-Fermi levels for trapped electrons and trapped holes respectively. The energies E_{fnt} and E_{fpt} correspond to the energy levels E_t where a trapped electron (hole) has the same probability of being emitted to the conduction (valence) band than to recombine with a hole (electron) of the valence (conduction) band.

The Eqs. ((7)–(8)) resemble the form of the Fermi–Dirac function. The equilibrium Fermi level is replaced by the trapped quasi-Fermi levels and there is a pre-factor that is absent in the Fermi–Dirac statistics. The main characteristic of the Simmons–Taylor occupation function $f(E_t)$ is that f is a smooth function with two steps [2]. Going from the valence towards the conduction band edge f decreases from 1 to the pre-factor of Eqs. ((7)–(8)) around E_{fpt}, and from this pre-factor to 0 around E_{fnt}; being approximately constant between E_{fpt} and E_{fnt} few kTs away of them. Similarly the recombination rate can be approximated by [3]:

$$R(E) = N_t(E)v_{th}\frac{\sigma_n\sigma_p np}{n\sigma_n + p\sigma_p}\left[1 + \exp\left(\frac{E_t - E_{fnt}}{kT}\right)\right]^{-1} \text{ for } E_t > E_{t0} \quad (9)$$

$$R(E) = N_t(E)v_{th}\frac{\sigma_n\sigma_p np}{n\sigma_n + p\sigma_p}\left[1 + \exp\left(\frac{E_{fpt} - E_t}{kT}\right)\right]^{-1} \text{ for } E_t < E_{t0} \quad (10)$$

In these equations only the traps located between the quasi-Fermi levels for trapped carriers E_{fpt} and E_{fnt} are acting as recombination centers.

In the Simmons and Taylor 0 K Approximation (0KSTA) the electron occupation function f is approximated by 0 at energies $E_t > E_{fnt}$ and by 1 at energies $E_t < E_{fpt}$. Therefore, the hole occupation functions $1 - f$ results 0 for $E_t < E_{fpt}$ and 1 for $E_t > E_{fnt}$. Hence both occupation functions f, $1 - f$ and the recombination rate R show abrupt transitions at the quasi-Fermi levels for trapped charges becoming double step functions:

$$f(E_t) = \begin{cases} 1 & \text{for } E_V < E_t < E_{fpt} \\ \dfrac{n\sigma_p}{n\sigma_n + p\sigma_p} & \text{for } E_{fpt} < E_t < E_{fnt} \\ 0 & \text{for } E_{fnt} < E_t < E_C \end{cases} \quad (11)$$

$$R(E_t) = \begin{cases} 0 & \text{for } E_V < E_t < E_{fpt} \\ N_t(E)v_{th}\dfrac{np\sigma_n\sigma_p}{n\sigma_n + p\sigma_p} & \text{for } E_{fpt} < E_t < E_{fnt} \\ 0 & \text{for } E_{fnt} < E_t < E_C \end{cases} \quad (12)$$

Hence the total recombination results as:

$$R = v_{th}\frac{np\sigma_p\sigma_n}{n\sigma_n + p\sigma_p}\int_{E_{fpt}}^{E_{fnt}} N(E)dE \quad (13)$$

The trapped charge concentration in acceptor- and donor-like traps becomes:

$$\rho = -q\left(\int_{E_V}^{E_{fpt}} N(E)dE + \frac{n\sigma_n}{n\sigma_n + p\sigma_p}\int_{E_{fpt}}^{E_{fnt}} N(E)dE\right) \quad (14a)$$

$$\rho = +q\left(\frac{p\sigma_p}{n\sigma_n + p\sigma_p}\int_{E_{fpt}}^{E_{fnt}} N(E)dE + \int_{E_{fnt}}^{E_C} N(E)dE\right) \quad (14b)$$

3. Methodology

Our simulations were performed with the computer code D-AMPS (Analysis of Microelectronic and Photonic Devices) that solves the system of three non-linear equations with the finite differences method and the Newton–Raphson method: Poisson's equation and continuity equations for free electrons and holes [6]. The independent variables are the electron potential and the quasi-Fermi levels. D-AMPS is an updated version of the well-known software AMPS released by the Pennsylvania State University that includes extra features like amphoteric states, the Defect Pool-model, the Pool–Frenkel effect, a simplified treatment of light scattering, etc.

The basic device that was initially selected to evaluate the accuracy of the STA approximation with D-AMPS was the a-Si:H based p–i–n junction. Our code was appropriately calibrated by fitting the measured dark and light current–voltage (J–V) characteristic curves. Samples were deposited in a multi-chamber RF-PECVD deposition facility and characterized with appropriate equipment at Delft University of Technology. The device structure is as follows: TCO/p-a-SiC:H/i-a-Si:H/n-a-Si:H/Al with a 5 nm thick silicon carbide buffer layer between the p- and i-layers. The front contact is an Asahi U-(SnO₂:F) type substrate with a textured surface. The p- and n-layer thicknesses are 10 nm and 20 nm, respectively. The Al back contact is 300 nm thick. The selected data correspond to a-Si:H based p–i–n junctions with intrinsic layer thicknesses of 200 and 600 nm.

The optical parameters were obtained from measured reflection and transmission spectra on a-Si:H films. The global density of states and the Urbach slope were extracted with the Dual Beam Photoconductivity. The other electrical input parameters were conveniently adjusted to reproduce the experimental data. The Uniform Density Model (UDM) that assumes a constant DB density in each device layer was adopted to simplify the discussion. The density of deep states in the UDM is described by three Gaussian distributions, recognized as D^-, D^0 and D^+. The peak energy of these Gaussians and their standard deviations are listed in Table 2 together with the most significant parameters that were obtained from our fittings. The correlation energy U was assumed equal to 0.2 eV [10–12]. In the p- and n-layers the doping densities were adjusted in order to reproduce the experimental activation energies.

In the optical model the intensity, I, of the incident light was shared among N sub-beams with intensity I/N and with different incident angles. The model accounts for light scattering on rough surfaces by angles different from 90º with respect to the incident sub-beams. These angles can vary between a maximum and a minimum value that can be selected at each interface by the user. The total generation

rate $G(x)$ of electron–hole (e–h) pairs results from adding the e–h pairs generated by each sub-beam.

Figs. 2 and 3 show our fittings of the dark J–V characteristics measured at 40 °C, and the light J–V characteristics measured at room temperature and under AM1.5 illumination of the a-Si:H based p–i–n devices already described. A similar procedure was followed to model and fit J–V curves of μc-SI p–i–n devices. The resulting electrical parameters and fittings can be found in a previous publication [13].

The calculation of the trapped carrier concentrations and recombination rate with the algorithms derived by Simmons and Taylor (STA and 0KSTA approximations) were included in D-AMPS. The user can choose the appropriate formalism, i.e. SRH, STA or 0KSTA by just changing the value of a single input parameter. In the 0KSTA approximation the direct implementation of abrupt step transitions at the quasi-Fermi levels for trapped carriers lead us to some convergence problems and instabilities. To circumvent this drawback the step transitions were realized with high-order low- and high-pass Butterworth filters [14]. Our results became insensitive to the order n of the Butterworth filter for n higher than 20.

4. Results of Implementating the Sta and 0ksta Approximations

4.1. Simmons–Taylor approximation

The test of the STA approximation performed on the a-Si:H based p–i–n devices of Figs. 2 and 3 gave us excellent results: the predicted J–V and SR curves evaluated with the SRH and the STA formalisms were on top of each other. The accuracy of the STA was explored at forward and reverse voltages that are the operation situations of solar cells and optical detectors respectively. Under illuminated conditions the STA precisely reproduces the curves obtained with the SRH formalism but this is not the case for the reverse-bias dark J–V characteristics. Actually this results was expected because the STA was designed to approximate the description of trapping and recombination rates when the quasi-Fermi levels move away from the Fermi level at thermodynamic equilibrium towards the respective band edges driven by either generation of e–h pairs by illumination or by carrier injection when the device is forward biased.

Table 2
List of electrical input parameters resulting from fitting dark and light J–V curves. The meaning of the symbols are as follows: W is the layer thickness, E_G is the mobility gap, N_c and N_v are the effective density of states at the conduction and valence band respectively, μ_N and μ_P are the electron and hole mobilities, E_D and E_A are the valence and the conduction tail slopes, t_N and t_P are the cross sections for electrons and holes in tail states, D^-, D^0 and D^+ are the densities of states enclosed by the three Gaussians, E^-, E^0 and E^+ are the peak positions of these Gaussians, σ_D are the standard deviations, σ_N and σ_P are the cross sections for electrons an hole in mid-gap states. The superscript $+$, 0 and $-$ indicates the charge state of the cross sections.

| Parameters	p	i	N
W (nm)	10	200/600	20
E_G (eV)	1.9	1.72	1.72
Nc, Nv (cm^{-3})	3×10^{20}	2.5×10^{20}	3×10^{20}
μ_N (cm^2 V^{-1} s^{-1})	5	30	5
μ_P (cm^2 V^{-1} s^{-1})	1	3.5	1
E_D (meV)	80	45	50
E_A (meV)	30	25	30
t_N^+ t_P^- (cm^2)	1×10^{-15}	1×10^{-15}	1×10^{-15}
t_N^0 t_P^0 (cm^2)	1×10^{-17}	1×10^{-17}	1×10^{-17}
D^- (cm^{-3})	2.14×10^{18}	2×10^{15}	3.06×10^{18}
D^0 (cm^{-3})	1.07×10^{18}	1×10^{15}	1.55×10^{18}
D^+ (cm^{-3})	2.14×10^{18}	2×10^{15}	3.06×10^{18}
E_D^- (eV)	0.7	0.55	0.6
E_D^0 (eV)	1.0	0.85	0.9
E_D^+ (eV)	1.3	1.15	1.2
σ_D (eV)	0.13	0.13	0.13
σ_N^+ σ_P^- (cm^2)	2×10^{-14}	2×10^{-14} / 1.2×10^{-14}	2×10^{-14}
σ_N^0 σ_P^0 (cm^2)	2×10^{-16}	3×10^{-15} / 1.2×10^{-15}	2×10^{-16}
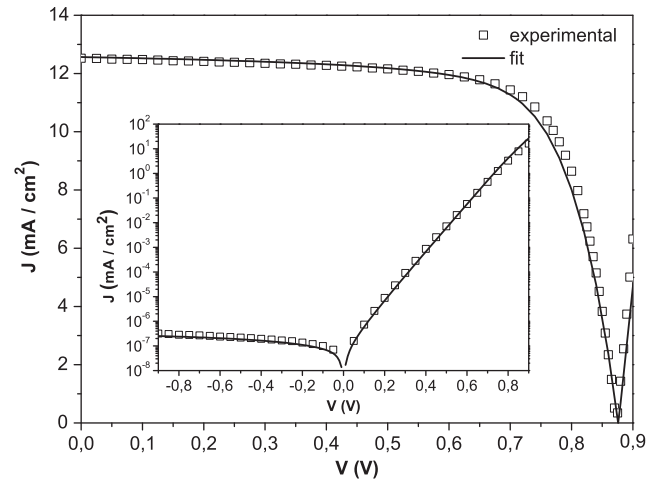
Fig. 2. Fitting of the experimental dark and light J–V characteristics of an a-Si:H based p–i–n junction with a 200 nm thick intrinsic layer.

Although the approximation was developed only for forward biased devices, it is interesting to check how the STA behaves when the same device is operating under reverse biased conditions. The dark J–V curves predicted by the STA were again compared using the SRH as a reference. Surprisingly the STA is still is able to reproduce quite well the shape of the dark J–V curve at reverse voltages, but overestimating the current by no more than 20%.

Our results for different temperatures for a-Si:H p–i–n device with a 600 nm thick intrinsic layer and for a μc-Si:H p–i–n device with a 1300 nm thick intrinsic layer at room temperature [13] are shown in Fig. 4a and b. Similar results are obtained for other intrinsic layer thicknesses and operating temperatures.

The dark current in a-Si:H based p–i–n is controlled at low-forward biases by recombination [15], at intermediate forward voltages but still inside the exponential region by a mixture of recombination and carrier diffusion, and at high forward voltages over the knee of the exponential the current is limited by the electron Space Charge Limited Current (SCLC) mechanism [16]. At these high voltages the virtual cathode limits the injection of electrons into the intrinsic layer. At reverse biases the current is controlled by thermal generation of electron–hole pairs. Under illumination and below the open circuit voltage (Voc) the current is defined by the difference between the photo-current and the recombination losses taking place in the intrinsic and doped layers. Under illumination but above Voc the SCLC mechanism also plays a role but the virtual cathode and anode
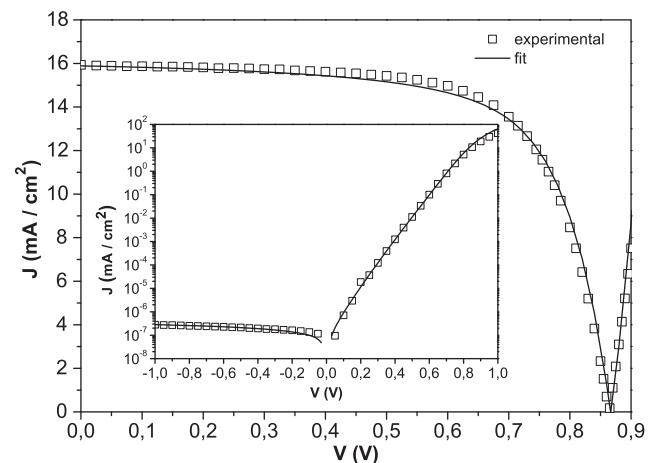

Fig. 3. Fitting of the experimental dark and light J–V characteristics of an a-Si:H based p–i–n junction with a 600 nm thick intrinsic layer.
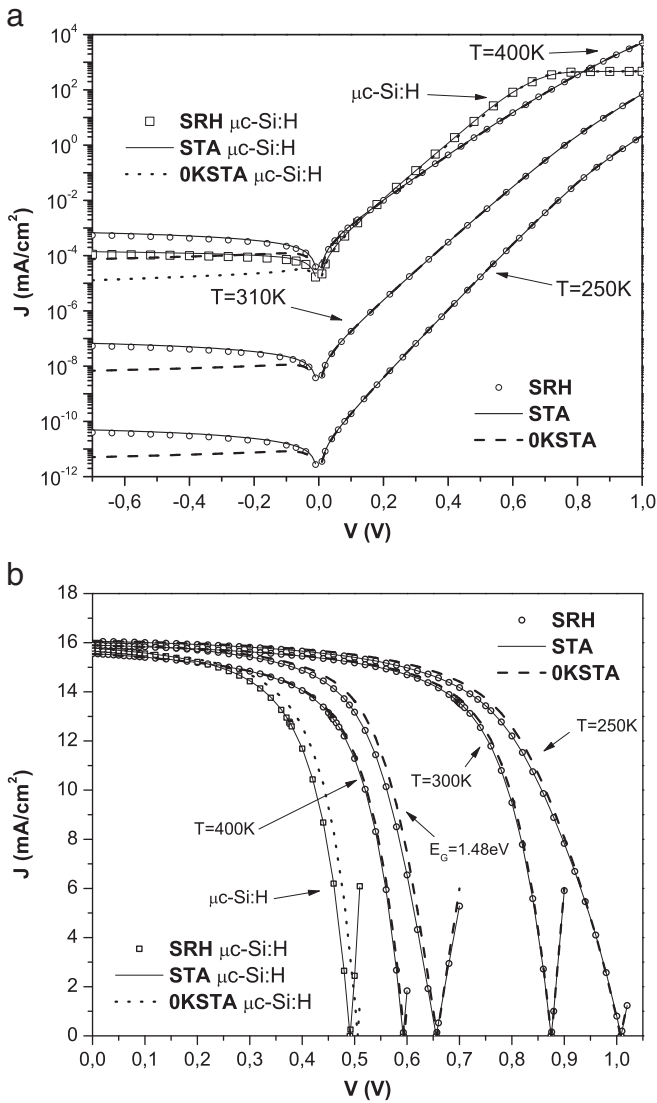
a

b

Fig. 4. Predicted J–V curves by D-AMPS (a) at dark condition for an a-Si:H p-i-n based device at different temperatures (250 K, 310 K, and 400 K) and for a μc-Si:H p-i-n junction at room temperature and (b) under AM1.5 illumination for an a-Si:H based device at different temperatures (250 K, 300 K, and 400 K), for an a-Si:H alloy p-i-n device with a mobility gap of 1.48 eV and for a μc-Si:H p–i–n device, the last two at room temperature. In both Figs. the a-Si:H mobility gap was assumed to be E_G = 1.72 eV. The J-V curves were evaluated with the SRH, STA, and 0KSTA formalisms. The intrinsic layer of the a-Si:H p-i-n device is 600 nm thick and the intrinsic layer of the μc-Si:H p-i-n device is 1300 nm thick. The J–V curves of the μc-Si:H p-i-n structure result from using the parameters of our reference [13].

are also tailored by the photo-generated carriers trapped along the whole device. Hence trapping and recombination have an important impact on the final shape of the dark and light J–V characteristics [16].

In Fig. 5 the recombination rate profiles evaluated with the SRH and STA formalisms are shown for different voltages under illuminated conditions. The recombination rate $R(x)$ is given in cm^{-3} s^{-1}; i.e. after the integration with respect to the density-of-states distribution in the band gap. The STA departs from the SRH equations only near the intrinsic trap level E_{t0} where either the neglected hole or electron emission coefficients are comparable. When we move further than few kTs from E_{t0} one of the two emission rates becomes negligible in the SRH formalism. Fig. 6a shows the band diagram of our 600 nm thick p–i–n device under dark conditions and with an applied forward voltage of 0.2 V. Besides the band edges and the quasi-Fermi levels for free carriers, this figure also shows the quasi-Fermi levels for trapped carrier and the intrinsic trap energy E_{T0} as defined by Simmons and Taylor.
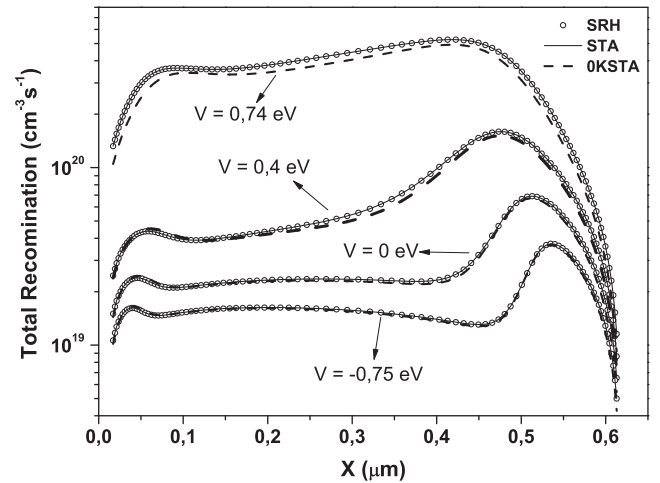

Fig. 5. Recombination rate profiles predicted by D-AMPS for an a-Si:H based device at 300 K under AM1.5 illumination and at different voltages. The intrinsic layer is 600 nm thick. Only the recombination rate profile in the intrinsic layer is shown.

It can be observed that the regions where recombination dominates over re-emission back into the bands is quite well defined in the bulk by the quasi-Fermi levels, but when either the p/i or the i/n interfaces are approached the energy range in which recombination takes place becomes much wider than the energies enclosed by the quasi-Fermi levels. When the device is illuminated, and either a forward or a reverse voltage is applied, or when the device is operating under dark conditions and a forward voltage is applied, the energy range in the band gap where capture rates are favored over the emission rates in the SRH formalism becomes wider. For instances Fig. 6b shows the band diagram of a device under AM1.5 illuminated and subjected to a small forward voltage. The higher the applied forward bias or the more intense the illumination intensity of the light source the wider the energy range where the emission rates are smaller than the capture rates. Hence the trapped carrier concentrations and the recombination rates are well reproduced by the STA, because the energy E_{T0} is located well inside the region where the emission rates are clearly smaller than the capture rates. Only when the forward applied voltage is very low (i.e., near the scenario of thermodynamic equilibrium) or when the applied voltage is reverse and the device operates under dark conditions or under low light intensities the neglected emission rate in the STA could lead to some errors. To be more specific the J–V curve predicted with the STA departs from the one resulting from the SRH formalism at flux intensities below 8x10^9 photons/cm^2/s when a red bias light (cut-off wavelength λ_C of ~ 0.68 μm) is impinging on the front contact as can be seen in Fig. 7. At very low forward voltages the region where the emission are not correctly evaluated is quite narrow (~ 0.01 V) leading to a departure of the dark J–V curve of at most 5%.

Under dark conditions and when a forward bias is applied to the device or under illuminated conditions, the electron quasi-Fermi level positions is above the hole quasi-Fermi level. On the other hand at reverse biases thermal generation of electron–hole (e–h) pairs is associated with inverted quasi-Fermi levels, i.e. the electron quasi-Fermi level is *below* the hole quasi-Fermi level. Interestingly as it can be seen in Fig. 8 the quasi-Fermi levels for trapped charge are also inverted, but only in the region where thermal generation of e–h pairs is really taking place and not in the whole device as the quasi-Fermi levels are. In this region of the intrinsic layer the emission rates are larger than the capture rates (see Fig. 8). The level E_{T0} crosses the region of inverted trapped quasi-Fermi levels. By neglecting one of the emission rates (for holes below E_{t0} and for electrons above E_{T0}) the occupation of traps that are located between the inverted quasi-Fermi levels for trapped charge is altered (see Eqs. (7) and (8)). For instance the occupation of traps by electrons
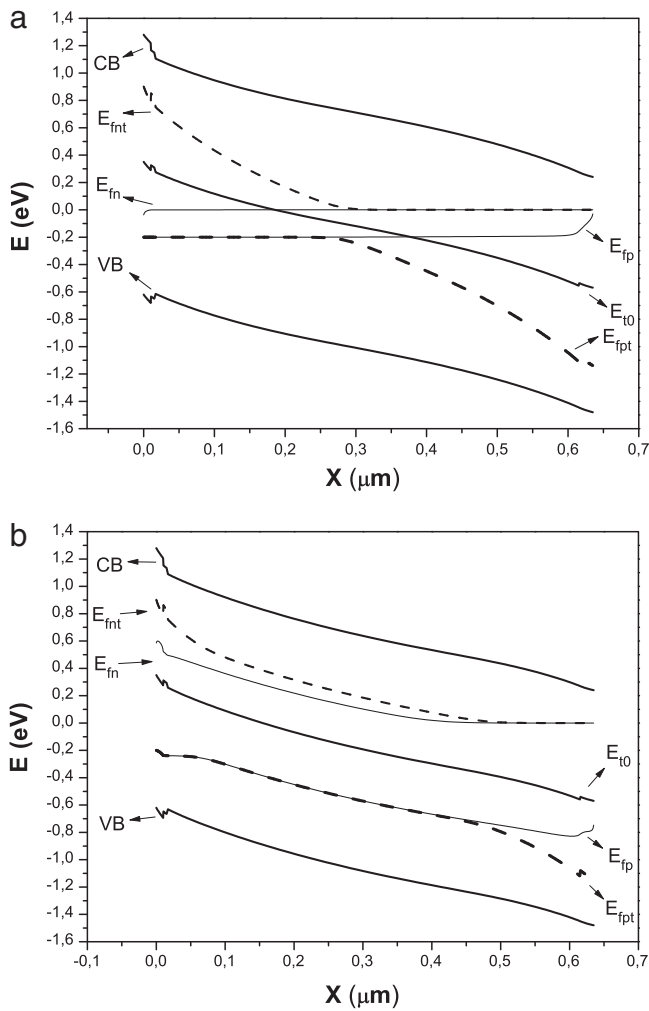
a

b

Fig. 6. Band diagram predicted by D-AMPS for an a-Si:H p-i-n based device (a) at dark conditions and (b) under AM1.5 illumination conditions. In both Figs. The device is operating at room temperature and subjected to a forward voltage of 0.2 V. The intrinsic layer is 600 nm thick. The quasi-Fermi levels, the quasi-Fermi levels for trapped carriers, and the intrinsic trap level E_{t0} for the trap species of acceptor-like deep states (Gaussians) are shown. CB and VB are the conduction and valence band respectively.

is overestimated by the STA below E_{T0} because the emission of electrons to the conduction band is forbidden. Simultaneously the occupation of traps by electrons is underestimated above E_{T0} by the STA because holes that are not allowed to be emitted to the valence band are lowering the occupation of traps by electrons. Similar statements can be made about holes. The net result is that more electrons in the traps above E_{T0} and more holes in the traps below E_{T0} are promoted to the conduction and valence bands by the STA approximation given rise to a higher dark current than the SRH formalism. Detailed simulations that are not included in this paper indicate that higher thermal generation rates are predicted by the Simmons–Taylor approximation at all localized gap states (either donor-like or acceptor-like, shallow or deep states).

In order to see how general these result could be the differences in the predicted device characteristic by D-AMPS with the SRH and STA formalisms on different a-Si:H p-i-n based scenarios were explored: higher and lower temperatures, thicker intrinsic layers, alloys with several mobility gaps and μc-Si:H structures. Our results indicate that the difference between the SRH and STA is still remarkably small when the p-i-n junction is subjected under illumination to either forward voltages or reverse voltages and under dark conditions when the p-i-n junction is subjected to forward voltages only. The comparisons were made for different intrinsic layer thicknesses,
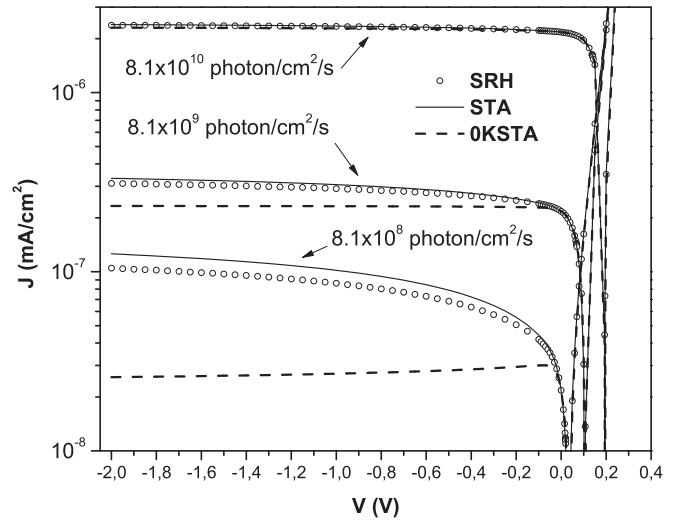

Fig. 7. Predicted J–V curves by D-AMPS using the SRH, STA, and 0KSTA formalisms for an a-Si:H based device illuminated by different bias light intensities. The bias light is red with a cut-off wavelength of 680 nm. The intrinsic layer is 600 nm thick.

temperatures, mobility gaps, and charged and neutral cross sections. We covered a temperature range of 250 K–400 K, mobility gaps from 1.45 eV to 2.0 eV, that can be found in a-Si:H and its alloys samples, (μc-Si:H p-i-n devices with a mobility gap of 1.25 eV gap were also inspected), intrinsic layer thicknesses between 500 nm and 3000 nm and different charged and neutral cross section ratios (100–0.01). Smaller gaps and higher temperatures increase the recombination losses. Higher kTs, increase the energy range around intrinsic trap level E_{T0} where the STA approximation could be questionable [3]. However, the STA algorithm still performs very well for any temperature, mobility gap, cross section ratios (even assuming neutral cross sections higher than charged cross sections), and intrinsic layer thicknesses inspected in this paper.

Using the parameters obtained from our fittings of J–V curves in p–i–n devices we have also explored the accuracy of the STA in single injection devices. These devices result an interesting test for the STA because as recombination is negligible the J–V and SR curves are only sensitive to carrier trapping. Also in single injection devices, like n–i–n, p–i–p structures, one junction is forward biased while the other junction is reverse biased for any applied external voltage.
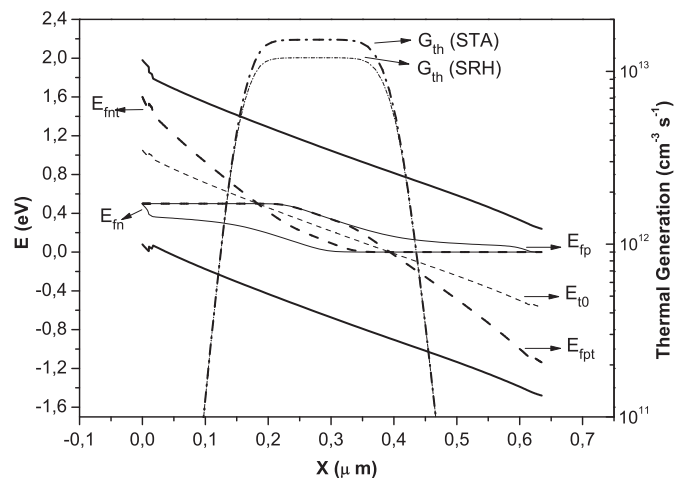

Fig. 8. Thermal generation and band diagram predicted by D-AMPS for an a-Si:H based device at room temperature and dark conditions and with a reverse voltage of 0.5 V. The intrinsic layer is 600 nm thick. The quasi-Fermi levels, the quasi-Fermi levels for trapped carriers, and the intrinsic trap level E_{T0} for the trap species of acceptor-like deep states (Gaussians) are shown.

However similar results were obtained for the predicted dark and light J–V when the SRH equations or the STA approximation were implemented. Our results are shown in Fig. 9.

The spectral responses (SR) of double injection devices is also well reproduced by the STA, because the incident light used in these measurements open the quasi-Fermi levels guarantying that recombination prevails over emission near E_{T0}.

4.2. Simmons–Taylor 0 K approximation

The 0KSTA assumes abrupt steep transitions at the trapped quasi-Fermi levels. The considerable simplifications obtained in the calculation and interpretation of the J–V curves [3] is accompanied by higher risks of introducing significant errors in the simulations [4,5].

Our results indicate that the 0KSTA still gives rise to acceptable dark J–V curves when the p–i–n device is forward biased (see Fig. 4a). Under AM1.5 illumination the 0KSTA slightly overestimates the current density J at already small forward voltages as result of underestimating the recombination rate when compared to the predictions obtained with the SRH formalism adopted as reference. Near the short circuit conditions the current densities predicted by the SRH and 0KSTA are quite similar but differences become visible near the maximum power point and also around Voc in µc-Si:H samples that leads to some errors in the estimation of FF and Voc. Higher forward voltages weaken the internal electric field inside the intrinsic layer that in turn increases the time that the photo-generated carriers remain in the device before being collected at contacts. This scenario favors the recombination at gap states located a bit outside of the energy region delineated by the quasi-Fermi for trapped carriers becoming non-negligible. The 0KSTA approximation ignores the contribution of these states (see Eq. (12)). In the SRH formalism states near the quasi-Fermi levels for trapped carriers make a non-negligible contribution to the recombination especially in semiconductors with lower mobility gaps where the quasi-Fermi levels for trapped carriers come closer to the band edges. States between the valence band edge and the quasi-Fermi level for trapped holes are able to capture a non-negligible amount of electrons from the conduction band that contribute to the overall recombination. Similarly, but to a less extent, states between the conduction band edge and the quasi-Fermi level for trapped electrons are able to capture holes from the valence band that also contribute to the overall recombination. Hence the 0KSTA leads to an underestimation of the recombination rate (see Fig. 5). However our results indicate that in p–i–n junction

with mobility gaps above 1.7 eV that are subjected to AM1.5 illumination the 0KSTA approximation can be considered still acceptable. A departure of the SRH model by no more than 4% in the predicted current when the mobility gap is 1.72 eV or higher was found in the scenarios studied in this paper.

At reverse-bias voltages the dark J–V predicted by the 0KSTA show significant and unacceptable errors in all cases that were studied (see Fig. 4). The thermal generation rates predicted inside the intrinsic layer by the 0KSTA are misleading. Fig. 8 shows that Eq. (12) selects regions located closer to the p/i and i/n interfaces where a net recombination is occurring. The 0KSTA is not able to detect in the intrinsic layer bulk the region where thermal generation of e–h pairs is really taking place because the quasi-Fermi levels for trapped carriers become inverted in energy and the 0KSTA sees a null net generation rate. On the other hand the STA formalism, that does not contain the approximation of sharp energy transitions at the quasi-Fermi levels for trapped carriers, is able to recognize this region where thermal generation is taking place. Actually the STA also accounts for the net recombination occurring near the interfaces but they are lower in comparison with the thermal generation present in the bulk. Fig. 9 shows that under low light level illumination the 0KSTA give rise to errors for flux intensities below 8×10^{10} photons/cm²/s when a red bias light is shining on the front contact ($\lambda_C \sim 0.68$ µm).

The 0KSTA leads also to inaccurate predictions of the J–V characteristics in single injection devices like n–i–n and p–i–p structures under either dark or illuminated conditions. The fact that one junction is always reversed biased for any external applied voltage plays against the accuracy of the 0KSTA approximation. Our results are shown in Fig. 8.

5. Conclusions

The Simmons–Taylor approximation (STA) can be used to simplify the description of the electrical transport in solar cells and optical detectors without losing accuracy. The current–voltage characteristics and spectral responses of double injection devices are quite well reproduced under illuminated conditions for any applied voltage and under dark conditions when the device is forward biased. The STA is found to be acceptable for a wide range of temperatures, intrinsic layer thicknesses and mobility gaps. The STA only overestimates by no more than 20% the current of double injection devices at reverse biases but properly reproduces the shape of the current–voltage curve. In detectors operating under low-light level illuminated conditions this error decreases when the light intensity increases and entirely vanishes at intensities of ~ 10^{10} photons/cm²/s or higher. The STA formalism also predicts current–voltage characteristics of single injection devices in good agreement with the SRH model under either dark or illuminated conditions for either positive or negative voltages. The "0 K" STA (0kSTA) can also be used in device modeling under similar restrictions to the ones found for the STA but taking some extra precautions. The 0KSTA overestimates the Fill Factor especially in solar cells with low mobility gap intrinsic layers and/or when they operate at lower temperatures. The 0KSTA also leads to important errors in the evaluation of current–voltage characteristics of single injection devices and it is entirely unacceptable when a double injection device is reversed biased and operates under dark conditions. Under low-level illumination the approximation becomes unacceptable below intensities of ~ 10^{11} photons/cm²/s.
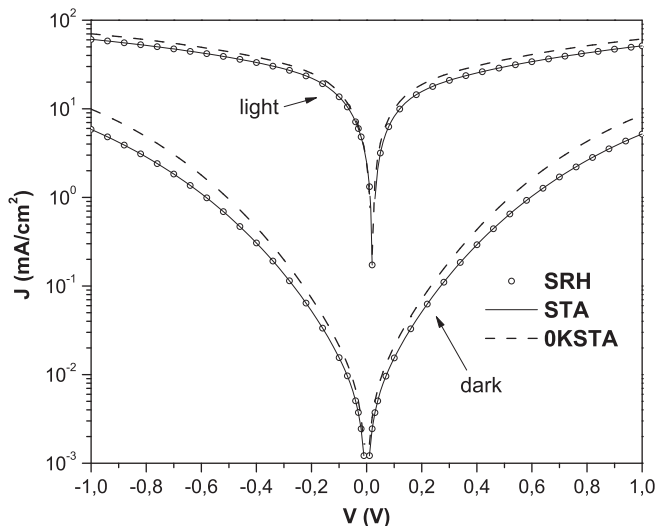

Fig. 9. Predicted dark J–V curves and light J–V curves (under AM1.5 illumination) by D-AMPS for an a-Si:H p–i–p device using the SRH, STA, and 0KSTA formalisms. The intrinsic layer is 600 nm thick. The characteristic curves obtained for a-Si:H n–i–n devices are similar.

References

[1] R.N. Hall, Phys. Rev. 87 (1952) 387.
[2] J.G. Simmons, G.W. Taylor, Phys. Rev. B 4 (2) (1971) 502.
[3] J.A. Willemen, Modelling of Amorphous Silicon Single- and Multi-Junction Solar Cells, (Ph. D. thesis) Delft University of Technology, 1998.
[4] M. Hack, M. Shur, J. Appl. Phys. 58 (2) (1985) 997.
[5] J.L. Gray, IEEE Trans. Electron Devices 36 (5) (1989) 906.
[6] Meinolf Block, Fachbereich Physik der Phillips-Universität Marburg, (PhD thesis), 1993.
[7] F. Rubinelli, J. Rath, R. Schropp, J. Appl. Phys. 89 (2001) 4010.
[8] R.N. Hall, Phys. Rev. 83 (1951) 228.
[9] W. Shockley, W.T. Read, Phys. Rev. 87 (5) (1952) 835.
[10] M. Powell, S. Deane, Phys. Rev. B 48 (1993) 10815.
[11] M. Powell, S. Deane, Phys. Rev. B 53 (1996) 10121.
[12] G. Schumm, Phys. Rev. B 49 (1994) 2427.
[13] J. Strengers, F.A. Rubinelli, J.K. Rath, R.E.I. Schropp, Thin Solid Film 501 (2006) 291.
[14] R.C. Gonzalez, R.E. Woods, Digital Image Processing, Second edition Prentice Hall, New Jersey, 2002.
[15] F. Rubinelli, J. Arch, S. Fonash, J. Appl. Phys. 72 (1992) 1621.
[16] F.A. Rubinelli, H. Liu, C.R. Wronski, Philos. Mag. B 74 (1996) 407.